SURFACES,
ELECTRON AND ION EMISSION

Magnetic Properties of 3d-Metal Nanocrystalline Films

G. I. Frolov

Kirenskiĭ Institute of Physics, Siberian Division, Russian Academy of Sciences,
Akademgorodok, Krasnoyarsk, 660036 Russia
e-mail: SVA@iph.krasn.ru
Received December 16, 2003

Abstract—The problem of designing high-resistivity soft magnetic materials based on 3d-metal nanocrystalline films is discussed. To increase the electrical resistivity, nanogranular composites are proposed; they consist of superparamagnetic particles embedded into a dielectric matrix. To obtain the required soft magnetic properties in such composites, it is necessary to realize magnetic ordering due to the effects of magnetic interaction between nanoparticles. As an example, magnetic films that exhibit good high-frequency properties in a range up to several hundreds of megahertz are presented. © 2004 MAIK "Nauka/Interperiodica".

INTRODUCTION

The nanocrystalline state of materials is a topical cross-disciplinary scientific problem involving materials science, solid-state physics, and solid-state chemistry [1–4]. During the last 15 years, the interest in this problem has been substantially increased due to the fact that a decrease in the grain size (primarily, in metals) to $D < 10$ nm results in significant changes in the properties of nanoparticles. To study the parameters of nanocrystalline materials, it is necessary to take into account not only the properties of nanoparticles but also the interaction between them.

Nanocrystalline composites are applied in various fields of modern engineering for creating soft and hard magnetic materials [1, 5] and data media for magnetic-memory devices [6]. We already discussed the problem of data media in [7], and, in this work, we study the problems dealing with the development of soft magnetic nanocrystalline materials.

One may question the expediency of designing new materials if amorphous alloys have excellent soft magnetic properties. The point is that 3d metal-based amorphous alloys have high electrical conductivity and cannot be used at frequencies above the kilohertz range. Nanoparticles consist of a core and a shell—phases having different physical properties, which should naturally increase the resistivity of such nanocomposites. Therefore, soft magnetic nanocrystalline materials open opportunities for their application in high-frequency devices.

STRUCTURE–COERCIVITY CORRELATION IN NANOCRYSTALLINE MAGNETIC MATERIALS

In the mid-1960s, the soft magnetic properties of nanocrystalline materials were described in a number of reviews [5, 8]. It was noted in [5] that the authors of [9, 10] were the first to study the effect of annealing on the magnetic properties of amorphous tapes. The annealed samples consisted of magnetic grains separated by an amorphous phase, whose volume fraction in the composite was ~20%. To decrease the sizes of the magnetic particles, Cu and Nb were added to the alloy; an interesting dependence of the coercive force on the diameter of the magnetic particles was discovered.

However, to be more exact, it was shown in the mid-1970s that a decrease in the crystallite size in permalloy films caused a sharp decrease in the coercive force [11]. The magnetic properties of FeNi(SiO) films were studied depending on the dielectric concentration (Figs. 1, 2).
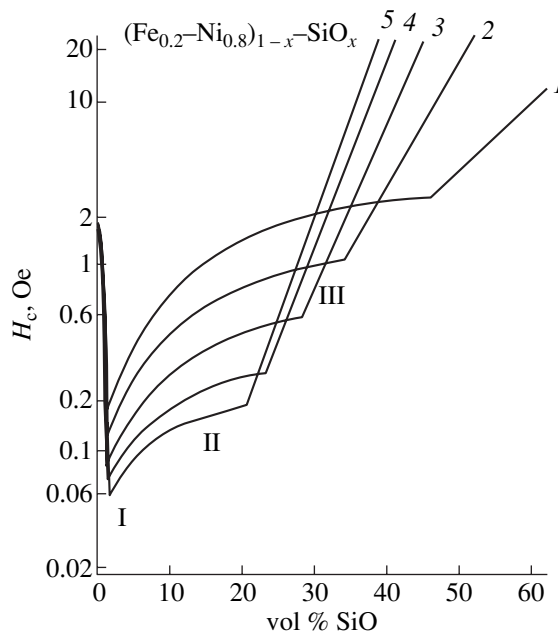

Fig. 1. Dependence of the coercive force in (Fe–Ni)–SiO films on the volume fraction of silicon monoxide. The film thickness is (*1*) 100, (*2*) 200, (*3*) 300, (*4*) 400, and (*5*) 500 nm.
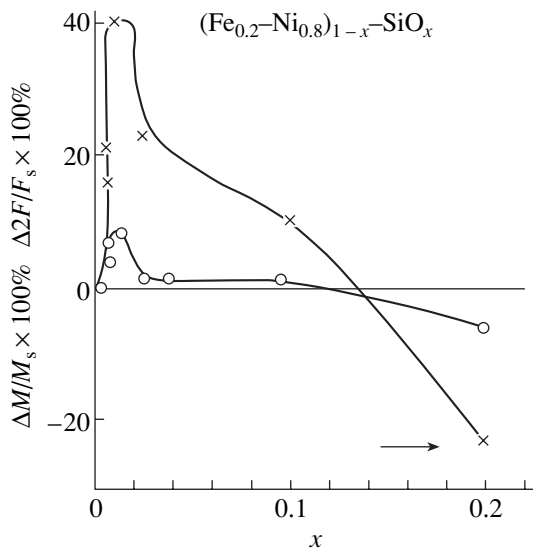
Fig. 2. Dependences of the relative changes in the saturation magnetization M_s and the Faraday rotation $2F$ in permalloy films on the volume fraction of silicon monoxide. $\bigcirc$, M_s; $\times$, $2F$.
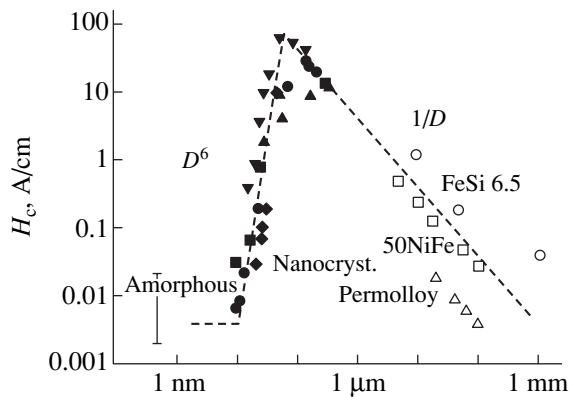

Fig. 3. Dependence of the coercive force on the grain size D in Fe-based nanocrystalline films. $T = 300$ K [8].

In this case, dielectric serves as a source of impurity states in the band structure of a metal and, on the other hand, increases the number of nucleation centers during condensation. In the former case, the introduction of a dielectric impurity modifies the electron spectra and, hence, changes the fundamental properties of the magnet [12]. In the latter case, it favors the formation of a nanocrystalline structure.

Experiments show that the composition range of permalloys for which relative changes in the magnetization and Faraday rotation are positive coincides with the range where these alloys have the properties of a strong ferromagnet. The concentration dependences of the saturation magnetization and the Curie temperature were simulated in [13]. An impurity (Si–O complexes) was assumed to penetrate into the permalloy lattice and to create a Coulomb potential that is caused by unsaturated valence bonds and is different from the potential of the unperturbed matrix. The screening of this charge by electrons of the d band, which has a higher density of states at the Fermi level, leads to changes in the fundamental magnetic parameters. However, the significant decrease in the coercive force H_c at ~2 vol % impurity (Fig. 1) was not explained. Electron-microscopic analysis shows that the crystallite size decreases to the values when a single-domain state is formed in crystallites. In this case, the main magnetization-reversal mechanism is rotation of the magnetic moment, which should increase the threshold magnetization-reversal fields [14].

These results, along with the data obtained in [9, 10], were explained in 1990 [15]. In the model proposed, the key factor of the dependence of the coercive force on the microstructure of a magnet is magnetic anisotropy and the possibility of controlling its value. The value of magnetic anisotropy mainly depends on the crystalline magnetic anisotropy K_1, which is determined by lattice symmetry. For $3d$ metals, K_1 is too high to reach low values of H_c. However, the effective contribution of K_1 can substantially be decreased by decreasing the grain size and taking into account the exchange interaction between grains.

According to the model of random anisotropy proposed to describe the properties of amorphous ferromagnets [16], the effective anisotropy K_{eff} in an ensemble of disoriented magnetic particles is determined by the ratio of the grain size D to the exchange-interaction radius

$$L_0 = \left(\frac{A}{K_1}\right)^{1/2},$$

where A is the interparticle exchange parameter.

At $D > L_0$, we have $K_{eff} = K_1 N^{1/2}$, where $N = (L_0/D)^3$. At $D < L_0$, $K_{eff} = K_1 N^{-1/2}$. Therefore, the dependence of H_c on the grain size has the form shown in Fig. 3 [8]. Three regions can be distinguished in this curve: in region I, where $D > L_0$, $H_c \sim 1/D$; that is, H_c increases with decreasing grain size; in region II, where $D = L_0$, $H_c = 2K_1/M_s$, where M_s is the saturation magnetization; and, in region III, where $D < L_0$, $H_c \sim D^6$. Figure 3 also shows the experimental data for Fe-based nanocrystalline materials, which confirm the calculation results.

Thus, we can assume that the model proposed correctly describes the experimental dependence of the coercive force on the particle size in nanocrystalline materials produced by annealing of amorphous samples. A specific feature of these materials is a particle size as small as ~10 nm. These materials can be applied at frequencies as high as several hundred kilohertz [5]. To use these materials at higher frequencies, their resistivity ρ must be increased.

One of the methods for solving this problem is the use of nanogranular condensates in which magnetic nanoparticles are embedded into a dielectric matrix.

However, the fraction of a dielectric layer should be low enough to retain good soft magnetic properties (high M_s). Therefore, the potential of this approach is limited by the probability of conduction-electron tunneling through a grain boundary [17]. To further increase ρ, one can use the dependence of the carrier density on the particle size. The authors of [18] showed that, when the particle size was smaller than the electron mean free path, some carriers were localized. The localization was found to affect the electrical conductivity more strongly than an increase in the scattering by boundaries, defects, and impurities. This effect was detected for 3d-metal nanoparticles with a size $D < 7$ nm.

Thus, to create high-resistivity nanocrystalline materials, one has to apply composites with a particle size <10 nm. Based on the model described above [8], the coercivity of such composites should be $H_c \approx 10^{-3}$ Oe. However, other values of H_c were detected experimentally. For example, in nanocrystalline Fe films with a particle size $D < 10$ nm, researchers found that $H_c = 30$ Oe in the films with $D = 6$ nm [19] and $H_c = 3$–5 Oe in the films with $D < 4$ nm [20].

Such a significant deviation from the calculated data can be due to the fact that the model assumed the independence of the main magnetic parameters of nanoparticles of their sizes. However, experiments show that the situation is different. As the value of D decreases, changes in the structure of nanoparticles increase the anisotropy constant and decrease M_s and A. For example, in the Fe films with $D = 6$ nm, $K = 2.5 \times 10^6$ erg/cm^3, $M_s = 850$ G, and $A = 10^{-7}$ erg/cm [19]. Thus, the exchange-interaction radius in these samples decreases as compared to the films with a particle size $D > 10$ nm and is equal to $L_0 = 5$ nm; i.e., $L_0 \approx D$. Then, to calculate H_c, we have to use the formula $H_c = 2K/M_s$; in this case, we obtain $H_c > 10^3$ Oe. This value is also inconsistent with the experimental data. This discrepancy indicates that a specific magnetic order is formed in 3d-metal films having a particle size <10 nm.

MAGNETIC HYSTERESIS IN NANOGRANULAR SYSTEMS WITH SUPERPARAMAGNETIC PARTICLES

To analyze the magnetic state of 3d-metal nanocrystalline films, let us turn to the results of [21], where the effects of thermal magnetization relaxation were studied in an ensemble of noninteracting single-domain particles having a uniaxial anisotropy. If this system is magnetized in a field H and the field is then removed, the remanent magnetization obeys the law

$$M_r = M_s \exp(-t/\tau), \qquad (1)$$

where t is the time after the field removal and τ is the relaxation time to the state of thermodynamic equilibrium.

The relaxation time is described by the expression

$$\tau = f_0 \exp(-KV/k_B T), \qquad (2)$$

where K is the uniaxial anisotropy constant; V is the particle volume; f_0 is the frequency factor, which is equal to the precession frequency of the magnetic moment of a particle ($f_0 = 10^9$ s^{-1}) in a first approximation; k_B is the Boltzmann constant; and T is the temperature. This exponential dependence results from the fact that the uniaxial-anisotropy energy of a particle depends on the angle between its magnetization and the easy axis. At $\tau/t \le 1$, the system changes to a superparamagnetic state ($M_r = 0$, $H_c = 0$).

Equation (2) can be used to determine the critical size V_{cr} of a particle at which it becomes superparamagnetic at $T = $ const or the temperature T_B of transformation of a particle into a superparamagnetic state at $V_{cr} = $ const.

At $\tau = 100$ s, which is the relaxation time characteristic of induction methods of measuring M_r, we find

$$V_{cr} = \frac{25k_B T}{K}, \quad T_B = \frac{KV}{25k_B}. \qquad (3), (4)$$

At $H = 0$, the threshold for the transformation of the system to a superparamagnetic state is $E = KV$. At $H \ne 0$, the threshold decreases and is given by

$$\Delta E(H) = KV\left[1 - \frac{HM_s}{2K}\right]^2. \qquad (5)$$

The coercive force of a particle at $T \ne 0$ is equal to the field at which the magnetization-reversal threshold $E(H)$ decreases to a value at which magnetization reversal occurs due to thermal effects in the experimental time t. Using Eqs. (3)–(5), we obtain [22]

$$H_c = H_{c_0}\left[1 - \left(\frac{V_{cr}}{V}\right)^{1/2}\right] = H_{c_0}\left[1 - \left(\frac{D_{cr}}{D}\right)^{3/2}\right], \qquad (6)$$

$$H_c = H_{c_0}\left[1 - \left(\frac{T}{T_B}\right)^{1/2}\right], \qquad (7)$$

where H_{c_0} is the coercive force of the particle at $T = 0$.

As follows from Eq. (6), the value of H_c decreases significantly as the nanoparticle size approaches D_{cr}. This dependence can be applied to produce nanocrystalline materials with a low coercive force. To this end, it is necessary to determine D_{cr} for 3d-metal nanoparticles.

Using the parameters of bulk materials, the authors of [21] obtained $D_{cr} \approx 20$ nm for α-Fe particles at $T = 300$ K. However, more recent studies showed that, as the particle size decreases, the particle structure changes to yield a core–shell system. As a result of restructuring, the uniaxial-anisotropy energy increases and D_{cr} decreases correspondingly. The experimental dependence of H_c on the core diameter of α-Fe nano-
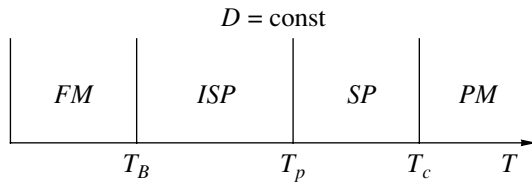
Fig. 4. Temperature dependence of the diagram for the magnetic state of an ensemble of nanoparticles (D = const).
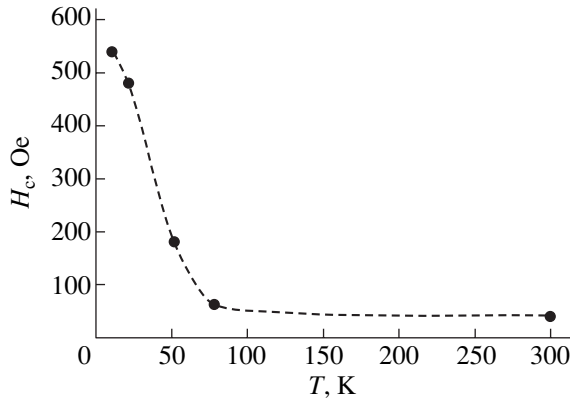

Fig. 5. Temperature dependence of the coercive force of Fe nanocrystalline films [19].

particles is given in [23]; at $T = 300$ K, particles with a core diameter of ~4 nm were found to transform into a superparamagnetic state ($H_c = 0$). An oxide shell around the core is ~2 nm thick. Therefore, for α-Fe nanoparticles, the critical diameter of the transformation to a superparamagnetic state at room temperature decreases to $D_{cr} \approx 6$ nm.

Thus, the data given above indicate that thermal effects cause a strong dependence of the coercive force on the magnetic-particle size. It should be noted that numerous experimental results obtained upon studying the properties of nanogranular magnetic materials formed by superparamagnetic particles have not been completely understood. For example, the appearance of magnetic hysteresis and magnetic ordering in an ensemble of superparamagnetic particles in the high-temperature limit ($T > T_B$) has not been interpreted [24]. Such effects are explained using several factors, such as a large scatter of particle sizes, the presence of a set of structurally or magnetically different phases, local anisotropy, and magnetic interaction between particles [25].

Therefore, one has to determine a factor that is predominant in the magnetic behavior of a nanogranular system in a certain particular case. In this respect, the experiments [26] on studying the effect of the interparticle distance on the magnetic properties of an ensemble of 3d-metal clusters placed in a nonmagnetic matrix are of interest. The authors provided constant nanoparticles sizes and structures and showed that, as the con-

tent of a magnetic phase decreased, the system is transformed from a magnetically ordered to a superparamagnetic state. This experiment indicates that the interparticle interaction substantially affects the magnetic state of the system.

Allia *et al.* [27] studied the effects of interparticle interaction and proposed a diagram of the magnetic state of an ensemble of nanoparticles depending on the particle size and temperature. The temperature dependence of this diagram is shown in Fig. 4.

At $T < T_B$, the system is in the ferromagnetic state. At $T > T_B$, the particles become superparamagnetic and the magnetic order remains unchanged (ISP region). According to [27], the magnetic energy of the ith particle that interacts with its neighbors can be written as

$$E = KV\sin^2\alpha + \sum K_m^{ij}M_i(T)M_j(T), \qquad (8)$$

where the first term on the right-hand side characterizes the uniaxial-anisotropy energy of the particle; the second term describes the energy of interaction between the particle and the nearest neighbors; M_i and M_j are the magnetization vectors of the ith and jth particles, respectively, and summation is carried out over all neighboring jth particles; and K_m^{ij} is the interparticle magnetic coupling constant.

Using the mean field theory, we can write

$$E = KV + K_mM^2(T)V. \qquad (9)$$

The temperature of transition from region FM to region ISP is $T_B = KV/25k_B$ (Fig. 5). At $T > T_B$, magnetic ordering in the system is formed due to the effects of magnetic interparticle interaction. In this case, the temperature of transition to the region of a superparamagnetic (SP) state is

$$T_p = \frac{K_mM^2(T)}{3k_B}. \qquad (10)$$

Region II on the diagram ($T_B < T < T_p$) has various names: the region of interacting superparamagnetic particles (ISP) [27] or the region of superferromagnetic ordering [28]. Since the contributions from the dipole–dipole and exchange interactions have not been exactly estimated, we prefer the name ISP. At $T > T_p$, the system transforms to the superparamagnetic state, and, at $T > T_C$, to the paramagnetic state (T_C is the Curie temperature). We now consider the behavior of the coercive force for the transitions described above. Figure 5 shows the experimental dependence $H_c = f(T)$ for α-Fe nanocrystalline films with a particle size of $D = 6$ nm [19]. Recall that, at $T = 300$ K, nanoparticles of this diameter should be paramagnetic. As is seen from Fig. 5, $H_c = $ const in a wide temperature range ($T = 70–300$ K), and, at $T < 70$ K, this dependence obeys Eq. (7); that is, $T_B = 70$ K for these films. Similar results were

obtained for Fe–SiO$_2$ films with a mean particle size of $D = 6$ nm [29].

To explain the unusual behavior of the $H_c = f(T)$ dependence in the ISP region (at $T > T_B$), we assume that magnetization only weakly depends on temperature here; hence, the interparticle magnetic interaction energy is constant. Therefore, $H_c = \text{const}$.

Thus, a magnetic order can be created in a system of interacting superparamagnetic particles; this order is characterized by a low coercive force and a weak temperature dependence of the coercive force. Since the 3*d*-particle size in this system is $D < 7$ nm, this system can have a high electrical resistivity.

MAGNETIC PROPERTIES OF HIGH-RESISTIVITY NANOGRANULAR FILMS

The idea of increasing resistivity in nanocrystalline materials by creating a dielectric layer between magnetic nanoparticles was realized in [30]; the authors studied the structure and magnetic properties of Fe–Sm–O films. The films were produced by reactive rf sputtering of an Fe target with Sm$_2$O$_3$ pellets on its surface in an Ar + O$_2$ atmosphere. The oxygen pressure was varied in the range 0–10% to produce films of various compositions. The structure, phase composition, and magnetic and electric properties of these films were studied (see table).

The film thickness was $d = 1$ μm. Electron-microscopic analysis showed that the films consisted of two phases: α-Fe nanocrystallites ($D = 10$ nm) and samarium oxide particles ($D = 3$ nm). The most interesting results were obtained for the Fe$_{83.5}$Sm$_{3.5}$O$_{13}$ film. The study of the frequency dependence of the quality factor ($Q = \mu_1/\mu_2$ is the ratio of the real to the imaginary component of magnetic permeability) showed that Q remained high up to $f = 40$ MHz.

The high-frequency magnetic properties of granular Co–Al–O films were studied in [31]. The films were produced by the same methods as in [30]; they consist of fcc Co particles with $D = 5$ nm surrounded by a dielectric Al–O layer. The properties of these films are the following: $d = 1.7$ μm, $M_s = 800$ G, $H_c = 5$ Oe, and ρ = 1100 μΩ cm. The frequency dependence of the magnetic permeability of the films was studied. The real part μ_1 of the magnetic permeability remains virtually constant up to $f = 500$ MHz and coincides with the calculated data. The high resistivity in these films is caused by a decrease in the size of magnetic nanoparticles to $D < 7$ nm and by the presence of a dielectric layer between them. The films produced represent a new class of high-frequency magnetic materials, which have a high value of μ_1 and a low value of μ_2 in a frequency range up to 200 MHz. A higher resistivity was realized in nanogranular Co–Sm–O films produced by the pulse-plasma evaporation of a Co$_5$Sm target in a

Table

PO$_2$, %	Composition	Saturation magnetization, G	Coercivity, Oe	Magnetic permeability ($f = 100$ MHz)	Electrical resistivity, μΩ cm
0	Fe$_{93}$Sm$_{3.5}$O$_{3.5}$	1570	13.7	153	40
2	Fe$_{87}$Sm$_4$O$_9$	1520	9	285	70
5	Fe$_{83.5}$Sm$_{3.5}$O$_{13}$	1430	0.8	2600	130
8	Fe$_{81}$Sm$_{3.5}$O$_{15.5}$	1330	8.5	550	170
10	Fe$_{56}$Sm$_3$O$_{41}$	310	24	44	240

vacuum of 10^{-6} Torr. This method of film deposition was described in [7].

In the initial state, the films are superparamagnetic ($T_B \approx 80$ K) and consist of Co particles ~2 nm in size surrounded by Sm$_2$O$_3$ layers. Annealing in a vacuum of 10^{-6} Torr changes the structure and properties of the films. Figure 6 shows the dependences of the resistivity, coercive force, and saturation magnetization on the annealing temperature. In the initial state, resistivity ρ of the films is equal to 5×10^{-2} Ω cm, which is about four orders of magnitude higher than the values characteristic of the corresponding metallic samples having a polycrystalline structure. The sharp decrease in ρ at $T_{ann} > 600$°C is caused by the destruction of the separating Sm$_2$O$_3$ interlayers and the formation of a galvanic contact between the metallic particles.

The variation of the coercive force with the annealing temperature is complex (Fig. 6b). Three regions with different values of H_c can be distinguished on this curve. Hysteresis loops that are typical of these regions are shown in Fig. 7. In region I, the loop becomes open only at $T < 80$ K, which indicates a superparamagnetic state of the samples. In region II ($T_{ann} = 200$–350°C), the loop becomes open at room temperature and has small values of H_c ($H_c = 0.1$–2 Oe, Fig. 7b). At $T_{ann} > 400$°C, H_c exhibits two specific features: it first increases jumpwise to 250 Oe and then increases to 450 Oe as a result of the second jump. Electron-microscopic analysis shows that, at these annealing temperatures, a polycrystalline structure is formed in the films and the sizes of Co particles increase by an order of magnitude. Note that, over the whole range of annealing temperatures, the saturation magnetization increases virtually threefold (Fig. 6c). Apparently, this effect is caused by not only structural factors but also phase transformations [32].

Figure 8 shows the temperature dependence of the coercive force for two films annealed at $T_{ann} = 250$ and 350°C in a constant magnetic field. Two segments can be distinguished on these curves: at low temperatures,
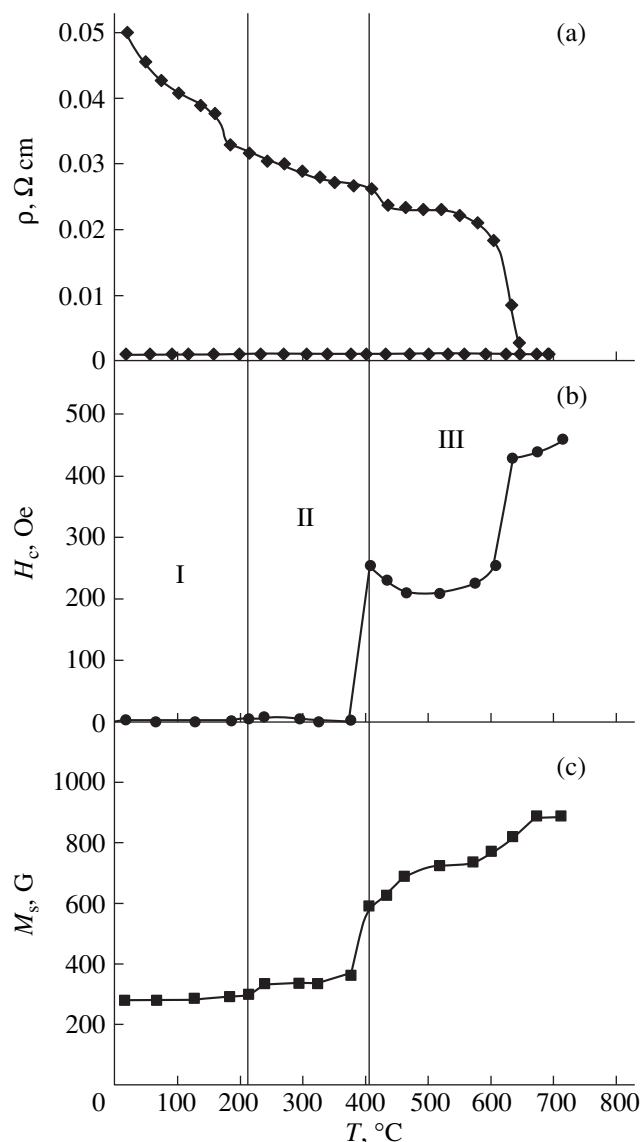
Fig. 6. Dependences of the (a) resistivity, (b) coercive force, and (c) saturation magnetization on the annealing temperature T_{ann} for Co–Sm–O films.

Fig. 7. Characteristic hysteresis loops for Co–Sm–O films (T = 300 K) (a) in the initial state and after annealing at T_{ann} = (b) 300 and (c) 480°C.

H_c exhibits a strong dependence, while at high temperatures, H_c is virtually unchanged. Performing $dM/dH = f(T)$ measurements, Zhao *et al.* [33] determined the blocking temperature. The transition between the first and second segments on the $H_c = f(T)$ dependence in Fig. 8 coincides with the T_B temperature. This result repeats the data given in Fig. 5. This finding allows the conclusion that the films annealed at T_{ann} = 250–350°C undergo the transition from the superparamagnetic state to the state of magnetic ordering of superparamagnetic particles (ISP region).

These results indicate that, indeed, an ensemble of interacting superparamagnetic particles can provide good magnetic properties at a high electrical resistivity.
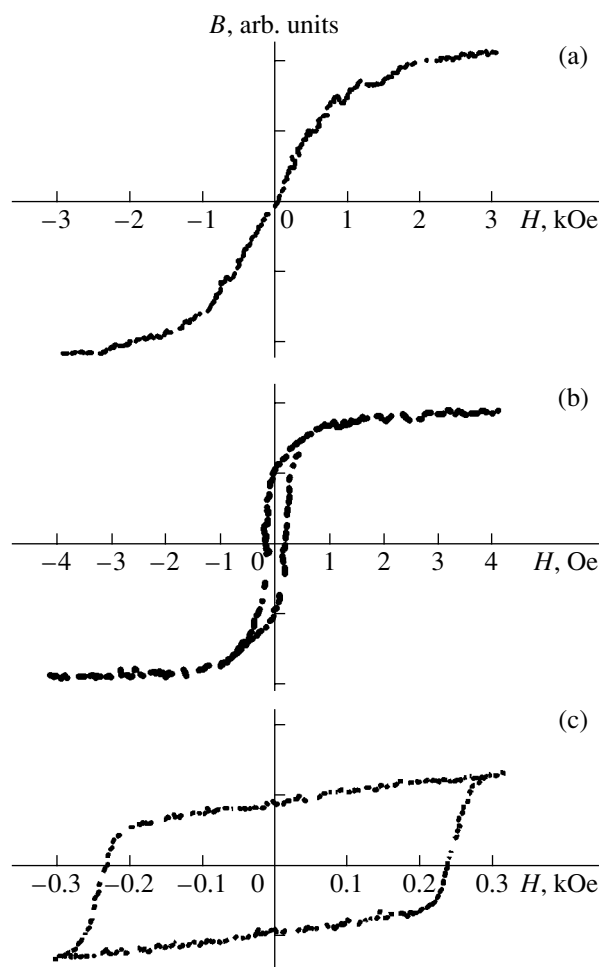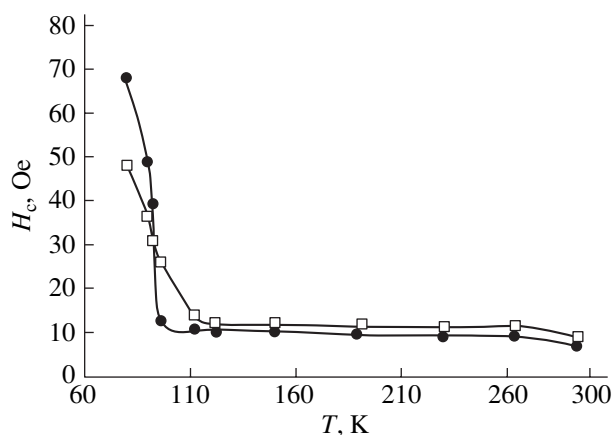

Fig. 8. Temperature dependence of the coercive force of Co–Sm–O films annealed at T_{ann} = 250 (●) and 350°C (□).

CONCLUSIONS

Analysis of the correlation between the microstructure and physical properties of nanocrystalline materials shows that 3d-metal granular films with a grain size <10 nm can provide a high resistivity, which offers the prospect of their application in microwave devices. The required soft magnetic properties in these materials can be ensured by the magnetic interaction between nanoparticles. The most interesting technological approach consists in the deposition of a film having a high content of a superparamagnetic phase at $T = 300$ K. Upon further annealing, the initial composite transforms into a specific state where magnetic ordering is realized but the particles remain superparamagnetic. The variation of the annealing temperature and the residual-gas pressure and the application of a constant magnetic field allow one to control the physical properties of such nanocrystalline films over a wide range.

REFERENCES

1. M. E. McHenry and D. E. Laughlin, Acta Mater. **48**, 223 (2000).

2. A. D. Pomogaĭlo, A. S. Rozenberg, and I. E. Uflyand, *Nanoparticles of Metals in Polymers* (Khimiya, Moscow, 2000).

3. A. I. Gusev and A. A. Rempel', *Nanocrystalline Materials* (Fizmatlit, Moscow, 2001).

4. S. P. Gubin and Yu. A. Koksharov, Neorg. Mater. **38**, 1287 (2002).

5. J. H. Vincent and S. P. S. Sangha, GEC J. Res. **13**, 2 (1996).

6. M. H. Kryder, W. Messner, and L. K. Garley, J. Appl. Phys. **79**, 4485 (1996).

7. G. I. Frolov, Zh. Tekh. Fiz. **71** (12), 50 (2001) [Tech. Phys. **46**, 1537 (2001)].

8. G. Herzer, Scr. Metall. Mater. **33**, 1741 (1995).

9. S. Y. Yoshizawa, S. Oguma, and K. Yamauchi, J. Appl. Phys. **64**, 6044 (1988).

10. S. Y. Yoshizawa, K. Yamauchi, T. Yamane, and H. Sugihara, J. Appl. Phys. **64**, 6047 (1988).

11. G. I. Frolov and V. S. Zhigalov, Fiz. Met. Metalloved. **40**, 518 (1975).

12. V. S. Zhigalov, Yu. M. Fedorov, and G. I. Frolov, Fiz. Met. Metalloved. **44**, 1303 (1977).

13. M. Sh. Erukhimov, V. S. Zhigalov, and G. I. Frolov, Fiz. Met. Metalloved. **49**, 1210 (1980).

14. E. C. Stoner and E. P. Wohlfarth, Philos. Trans. R. Soc. London, Ser. A **240**, 559 (1948).

15. G. Herzer, IEEE Trans. Magn. **26**, 1397 (1990).

16. R. Alben, J. J. Becker, and M. C. Chi, J. Appl. Phys. **49**, 1653 (1978).

17. G. Reiss, J. Vancea, and H. Hoffmann, Phys. Rev. Lett. **56**, 2100 (1986).

18. J. Vancea and H. Hoffmann, Thin Solid Films **92**, 219 (1982).

19. J. P. Perez, V. Dupuis, J. Tuaillon, *et al.*, J. Magn. Magn. Mater. **145**, 709 (1995).

20. G. I. Frolov, V. S. Zhigalov, L. I. Kveglis, *et al.*, Fiz. Met. Metalloved. **88** (2), 85 (1999).

21. C. P. Bean and J. D. Livingston, J. Appl. Phys. **30** (4), 120s (1959).

22. E. F. Kneller and F. E. Luborsky, J. Appl. Phys. **34**, 656 (1963).

23. S. Gandopadhyay, G. C. Hadjipanayis, B. Dale, *et al.*, Phys. Rev. B **45**, 9778 (1992).

24. P. Allia, M. Coisson, M. Knobel, *et al.*, Phys. Rev. B **60**, 12207 (1999).

25. *Proceedings of NMP Conference, Spain 1998*; J. Magn. Magn. Mater. **203** (1999).

26. V. Dupuis, J. Tuaillon, B. Prevel, *et al.*, J. Magn. Magn. Mater. **165**, 42 (1997).

27. P. Allia, M. Coisson, P. Tiberto, *et al.*, Phys. Rev. B **64**, 144420 (2001).

28. S. Morup, Europhys. Lett. **28**, 671 (1994).

29. B. J. Jonsson, T. Turrki, V. Strom, *et al.*, J. Appl. Phys. **79**, 5063 (1996).

30. T.-S. Yoon, Y. Li, W.-S. Cho, and C.-O. Kim, J. Magn. Magn. Mater. **237**, 288 (2001).

31. H. Fujimori, S. Mitani, and T. Matsumoto, J. Appl. Phys. **79**, 5130 (1996).

32. G. I. Frolov, V. S. Zhigalov, S. M. Zharkov, *et al.*, Fiz. Tverd. Tela (St. Petersburg) **45**, 2198 (2003) [Phys. Solid State **45**, 2303 (2003)].

33. B. Zhao, J. Y. Chow, and X. Yan, J. Appl. Phys. **79**, 6022 (1996).

Translated by K. Shakhlevich